Provided for non-commercial research and education use.
Not for reproduction, distribution or commercial use.

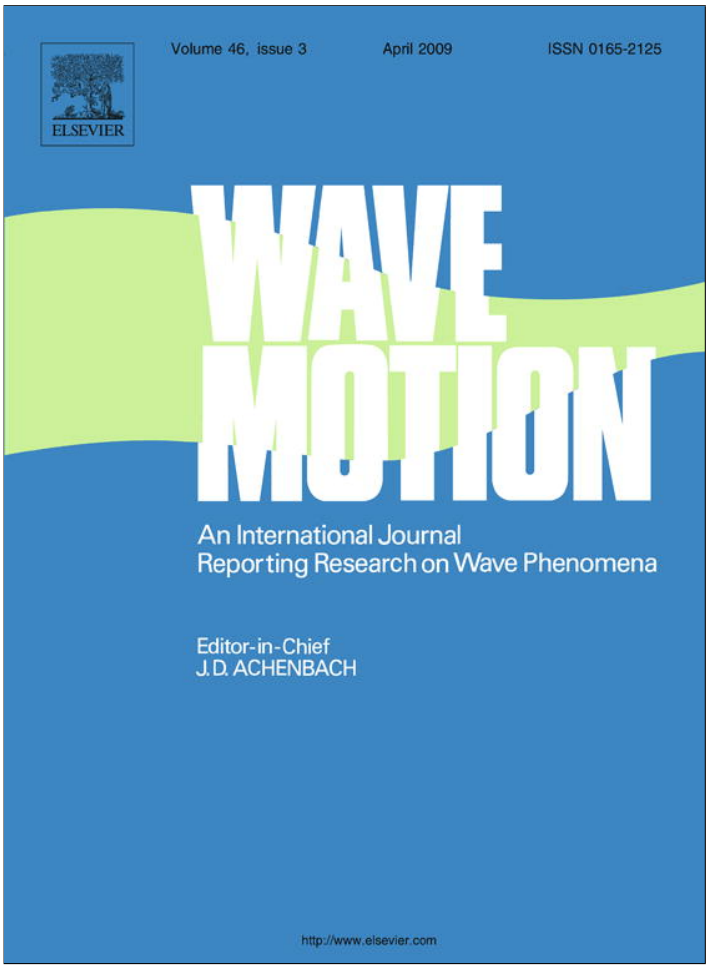

This article appeared in a journal published by Elsevier. The attached copy is furnished to the author for internal non-commercial research and education use, including for instruction at the authors institution and sharing with colleagues.

Other uses, including reproduction and distribution, or selling or licensing copies, or posting to personal, institutional or third party websites are prohibited.

In most cases authors are permitted to post their version of the article (e.g. in Word or Tex form) to their personal website or institutional repository. Authors requiring further information regarding Elsevier's archiving and manuscript policies are encouraged to visit:

http://www.elsevier.com/copyright

Author's personal copy

Wave Motion 46 (2009) 210–220

Contents lists available at ScienceDirect

Wave Motion

journal homepage: www.elsevier.com/locate/wavemoti

High-order non-reflecting boundary conditions for the linearized 2-D Euler equations: No mean flow case

John R. Dea [a], Francis X. Giraldo [b], Beny Neta [b,*]

[a] Department of Mathematics and Statistics, Air Force Institute of Technology, Wright-Patterson AFB, OH 45433, United States
[b] Department of Applied Mathematics, Naval Postgraduate School, Monterey, CA 93943, United States

ARTICLE INFO

Article history:
Received 24 March 2008
Received in revised form 3 November 2008
Accepted 25 November 2008
Available online 10 December 2008

Keywords:
Non-reflecting boundary conditions
Euler equations
Finite differences
Absorbing boundary conditions

ABSTRACT

Higdon-type non-reflecting boundary conditions (NRBCs) are developed for the 2-D linearized Euler equations with Coriolis forces. This implementation is applied to a simplified form of the equations, with the NRBCs applied to all four sides of the domain. We demonstrate the validity of the NRBCs to high order. We close with a list of areas for further research.

Published by Elsevier B.V.

1. Introduction

To perform mesoscale atmospheric modeling on a computer, one immediately runs into the problem of defining the computational domain. At some point, there has to be an edge to the computational domain, but the physical atmosphere lacks any edges. How, then, can we define a computational boundary where no physical boundary exists? The answer of course is to define a *non-reflecting* boundary condition (NRBC). How best to define such a boundary has been an active area of research for approximately 30 years. Ideally, an NRBC will be stable, accurate, fast, and easy to implement; realistically, one must generally choose two or three of those criteria, at best.

There are typically two approaches to NRBC development. The first is to prescribe the behavior at the boundaries in such a way as to reduce any spurious reflections. Early examples include the Sommerfeld-condition-based work of Orlanski [26] and the Padé approximations of Engquist and Majda [4,5]. This approach was expanded by Higdon [13–19] and subsequently automated by Givoli, Neta, and van Joolen [7–10,29–32]. The Orlanski scheme and the Engquist–Majda scheme are less accurate than their successors; however, the Higdon scheme and its offshoots suffer from very high computational overhead.

The second approach is to surround the domain with a more dispersive computational medium, so that incoming waves enter the absorbing layer and diffuse to zero before their reflections re-enter the original domain. Examples include the perfectly matched layer (PML) developed by Bérenger [1], applied to the linearized shallow water equations by Navon et. al. [24] and to the linearized Euler equations by Hu [20–22], and the sponge layer used by Giraldo and Restelli [6]. This approach requires additional storage and computation time for the expanded domain, and some reflections are still evident when the theoretically-exact absorbing layer is applied to a discrete computational domain.

Here we apply the Higdon scheme to the linearized Euler equations. We take advantage of the Givoli–Neta–van Joolen automation and make subsequent improvements to reduce the computational overhead. This method removes

* Corresponding author. Tel.: +1 831 656 2235; fax: +1 831 656 2355.
E-mail address: byneta@gmail.com (B. Neta).

0165-2125/$ - see front matter Published by Elsevier B.V.
doi:10.1016/j.wavemoti.2008.11.002

Author's personal copy

approximately 97% of the Sommerfeld-condition's reflection error with only a modest increase to the computational time.

The rest of the paper is organized as follows: In Section 2 we outline the problem under consideration, the linearized Euler equations in 2-D with no advection, solved in an infinite domain with NRBCs on all four sides. Section 3 details the NRBCs and their application to the linearized Euler equations. In Section 4 we derive the Klein–Gordon equation from the linearized Euler equations with no mean flow. We discuss the finite difference discretization for the NRBCs and the interior scheme in Sections 5 and 6, and we provide a numerical example in Section 7. We then list some areas for further research (Section 8) and summarize our results (Section 9).

2. Problem statement

Consider the linearized Euler equations in an open domain. For simplicity we assume that the domain has a flat bottom and that there is no advection, although this assumption may be removed in future studies. A Cartesian coordinate system (x, y) is introduced, as shown in Fig. 1.

The non-linear Euler equations are

$$\begin{aligned}
&\partial_t \rho + \partial_x(\rho u) + \partial_y(\rho v) = 0,\\
&\partial_t u + u\partial_x u + v\partial_y u + \frac{1}{\rho}\partial_x p = fv,\\
&\partial_t v + u\partial_x v + v\partial_y v + \frac{1}{\rho}\partial_y p = -fu,\\
&\partial_t p + u\partial_x p + v\partial_y p + \gamma p(\partial_x u + \partial_y v) = 0,
\end{aligned} \tag{1}$$

where we use the following shorthand for partial derivatives

$$\partial_a = \frac{\partial}{\partial a}, \quad \partial_{ab} = \frac{\partial^2}{\partial a \partial b},$$

and t denotes the time, $u(x, y, t)$ and $v(x, y, t)$ the unknown velocities in the x and y directions, $\rho(x, y, t)$ the density, $p(x, y, t)$ the pressure, f the constant Coriolis acceleration due to the Earth's rotation, and $\gamma = c_p/c_v$ the constant ratio of specific heats. Linearizing these equations about mean zero velocities, constant mean density ρ_0 and constant mean pressure p_0 (see, e.g., [20] or [23]), we get

$$\partial_t \rho + \rho_0(\partial_x u + \partial_y v) = 0, \tag{2a}$$

$$\partial_t u + \frac{1}{\rho_0}\partial_x p = fv, \tag{2b}$$

$$\partial_t v + \frac{1}{\rho_0}\partial_y p = -fu, \tag{2c}$$

$$\partial_t p + \gamma p_0(\partial_x u + \partial_y v) = 0. \tag{2d}$$

At $\vec{x} \to \infty$ the solution is known to be bounded and not to include any incoming waves. To complete the statement of the problem, initial values for u, v, p and ρ are given at time $t = 0$ in the entire domain.

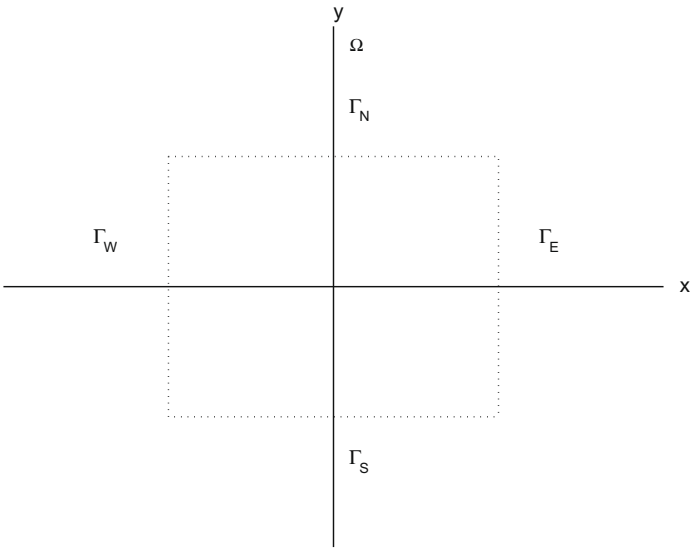

Fig. 1. An open domain Ω truncated by artificial boundaries Γ_N, Γ_W, Γ_S, and Γ_E.

Author's personal copy

We now truncate the infinite domain by introducing an artificial boundary Γ, with Γ_N located at $y = y_N$, Γ_W located at $x = x_W$, Γ_S located at $y = y_S$, and Γ_E located at $x = x_E$ (see dotted lines in Fig. 1). To obtain a well-posed problem in the finite domain Ω we need, instead of the condition at infinity, a single boundary condition on each of the artificial boundaries $\Gamma_{N,W,S,E}$. This should be a non-reflecting boundary condition (NRBC). We shall apply a high-order NRBC for the variables, as described in the following section.

3. Higdon-type NRBCs

On the artificial boundaries Γ we use one of the *Higdon NRBCs* [19]. These NRBCs were presented and analyzed in a sequence of papers [13,15–18] for non-dispersive acoustic and elastic waves, and were extended in [19] for dispersive waves. Their main advantages are as follows:

1. The Higdon NRBCs are very *general*, namely they apply to a variety of wave problems, in one, two, and three dimensions and in various configurations.
2. They form a *sequence* of NRBCs of increasing order. This enables one, in principle (leaving implementational issues aside for the moment), to obtain solutions with unlimited accuracy.
3. The Higdon NRBCs can be used, without any difficulty, for *dispersive* wave problems and for problems in stratified media. Most other available NRBCs are either designed for non-dispersive media (as in acoustics and electromagnetics) or are of low order (as in meteorology and oceanography).

The scheme used here is different than the original Higdon scheme [19] in the following ways:

1. The discrete Higdon conditions were developed in the literature up to third order only, because of their algebraic complexity which increases rapidly with the order. Givoli and Neta [8] showed how to easily implement these conditions to an *arbitrarily high order*. The scheme is coded once and for all for any order; the order of the scheme is simply an input parameter.
2. The original Higdon conditions were applied to the Klein–Gordon linear wave equation and to the elastic equations. Here we show how to apply them to the *linearized Euler equations* (2b).
3. The Higdon NRBCs involve some parameters which must be chosen. Higdon [19] discusses some general guidelines for their manual *a priori* choice by the user. Neta et. al. [25] showed how a simple choice for these parameters can dramatically simplify the calculations and enable implementation of NRBCs of much higher order with less computational overhead.

The Higdon NRBC of order J is

$$H_J: \quad \left[\prod_{j=1}^{J}(\partial_t + C_j\partial_x)\right]\eta = 0 \text{ on } \Gamma_E, \tag{3}$$

where η represents any one of the state variables ρ, u, v, p. Here, the C_j are parameters which have to be chosen and which signify phase speeds in the x-direction. The boundary condition (3) is exact for all waves that propagate with an x-direction phase speed equal to any of $C_1 \ldots C_J$. This is easy to see from the reflection coefficient (see below). For the boundary Γ_W we replace ∂_x by $-\partial_x$. Likewise, on $\Gamma_{N,S}$ we use $\pm\partial_y$. Givoli and Neta [8] and Dea et. al. [2] summarize several observations about these NRBCs, most of which we omit here for brevity. One point is worth repeating: For the Klein–Gordon equation, Higdon showed [19] that the *reflection coefficient* for an NRBC of order J can be given by

$$|R| = \prod_{j=1}^{J}\left|\frac{C_j - C_x}{C_j + C_x}\right|, \tag{4}$$

where C_x is the wave speed in the x direction. Note that this reflection coefficient is a product of J factors, each of which is less than one. Consequently, increasing the order J of the NRBC will result in reduced reflections, even if the C_j values are suboptimal. We will take advantage of this fact when we discuss the NRBC discretization in Section 5, where we show that a certain choice of C_j can reduce the computational complexity from $O(3^J)$ to $O(J^2)$.

4. Equivalence of linearized Euler equations and Klein–Gordon equation

Higdon showed in [19] that this NRBC formulation is compatible with the Klein–Gordon (dispersive wave) equation

$$\partial_t^2\eta - C_0^2\nabla^2\eta + f^2\eta = 0. \tag{5}$$

Hence, if we can show that (2b) is equivalent to (5), we can claim that this NRBC formulation will be stable here. Differentiate (2bd) with respect to t

$$\partial_{tt}p + \gamma p_0(\partial_{xt}u + \partial_{yt}v) = 0. \tag{6}$$

Author's personal copy

Now differentiate (2bb) with respect to x and (2bc) with respect to y and add

$$\partial_{xt}u + \partial_{ty}v + \frac{1}{\rho_0}\left(\partial_{xx}p + \partial_{yy}p\right) = f(\partial_x v - \partial_y u). \tag{7}$$

Now substitute (7) into (6)

$$\partial_{tt}p - \frac{\gamma p_0}{\rho_0}(\partial_{xx}p + \partial_{yy}p) + f\gamma p_0(\partial_x v - \partial_y u) = 0. \tag{8}$$

Differentiate (2bb) with respect to y and (2bc) with respect to x and subtract

$$\partial_{yt}u - \partial_{xt}v = f(\partial_y v + \partial_x u). \tag{9}$$

If we substitute this result into the time derivative of (8), removing the $\nabla \times \vec{u}$ term, and apply (2bd), we get an equation for $\partial_t p$, which we can integrate over time to get

$$\partial_{tt}p - \frac{\gamma p_0}{\rho_0}\nabla^2 p + f^2(p - p_0) = 0, \tag{10}$$

which gives us the Klein–Gordon equation for the pressure perturbation $p - p_0$ with wave speed $\sqrt{\gamma p_0/\rho_0}$.

5. Discretization of NRBCs

The Higdon condition H_J is a product of J operators of the form $\partial_t + C_j\partial_x$. Consider the following finite difference approximations (see e.g. [27]):

$$\partial_t \simeq \frac{I - S_t^-}{\delta t}, \quad \partial_x \simeq \frac{I - S_x^-}{\delta x}. \tag{11}$$

In (11), δt and δx are, respectively, the time-step size and grid spacing in the x direction, I is the identity operator, and S_t^- and S_x^- are backward shift operators defined by

$$S_t^-\eta_{pq}^n = \eta_{pq}^{n-1}, \qquad S_x^-\eta_{pq}^n = \eta_{p-1,q}^n. \tag{12}$$

Here and elsewhere, η_{pq}^n is the FD approximation of $\eta(x,y,t)$ at grid point (x_p, y_q) and at time t_n. We use (11) in (3) to obtain

$$\left[\prod_{j=1}^{J}\left(\frac{I - S_t^-}{\delta t} + C_j\frac{I - S_x^-}{\delta x}\right)\right]\eta_{\mathrm{Eq}}^n = 0. \tag{13}$$

Here, the index E corresponds to a grid point on the boundary Γ_E. On the other open boundaries, the normal derivatives and shift operators should be adjusted accordingly.

Givoli and Neta [8] showed how to implement the Higdon NRBCs *to any order* using a simple algorithm. Their algorithm requires the summation of $O(3^J)$ terms. However, if we make the simplification

$$C_j \equiv C_0 \quad \forall j \in 1 \ldots J, \tag{14}$$

then we can simplify the summation to

$$Z \equiv \left(aI + bS_t^- + cS_x^-\right)^J \eta_{\mathrm{Eq}}^n = \sum_{\beta=0}^{J}\sum_{\gamma=0}^{J-\beta}\frac{J!}{\alpha!\beta!\gamma!}a^\alpha b^\beta c^\gamma S_t^{-\beta}S_x^{-\gamma}\eta_{\mathrm{Eq}}^n = 0, \tag{15}$$

where

$$a = 1 - c,$$
$$b = -1,$$
$$c = -C_0\frac{\delta t}{\delta x},$$
$$\alpha = J - \beta - \gamma.$$

This summation consists of only $O(J^2)$ terms, reducing the computational time considerably. As shown in the discussion of the reflection coefficient in Section 3, this choice of C_j will be less accurate than an optimized selection of C_j's based on dispersive wave speeds; however, the results will still improve as we increase our order J. We accept the slight loss of accuracy in exchange for the significant increase in speed. Note also that the $J = 1$ case, with this choice of C_j, is the classic Sommerfeld radiation condition. We choose this particular NRBC wave speed as a middle ground between the phase speeds of the dispersive waves and the lowered normal velocities associated with non-zero incidence angles.

6. Discretization in the interior

We consider explicit FD interior discretization schemes for the linearized Euler equations (2b) to be used in conjunction with the H_J condition. The interaction between the H_J condition and the interior scheme is a source of concern, since simple

Author's personal copy

choices for an explicit interior scheme turn out to give rise to instabilities. The effort to contrive a compatible discretization scheme was described in [2] for the linearized Euler equations without Coriolis. There, we used a one-sided differencing scheme for the interior, such that the discretized system was equivalent to the standard second-order centered-difference scheme for the scalar wave equation in p, which Higdon proved in [19] was compatible with the NRBC formulation. However, subsequent work has shown that adding the Coriolis terms to this scheme results in a system which cannot be converted to the Klein–Gordon equation. Hence, another approach is needed.

Let us reconsider a second-order centered-difference (leap-frog) scheme,

$$\eta'(a) \approx \frac{\eta(a+\delta a) - \eta(a-\delta a)}{2\delta a}, \tag{16}$$

where η denotes any of our four state variables, and a denotes any of our spatial or temporal variables. Using the shift operator notation from the preceding section, we define our difference approximations as

$$\Delta_a = \frac{S_a^+ - S_a^-}{2\delta a}, \tag{17}$$
$$a \in \{x, y, t\}.$$

From this definition, we propose the following discretization scheme for (2b):

$$\Delta_t \rho + \rho_0(\Delta_x u + \Delta_y v) = 0, \tag{18a}$$
$$\Delta_t u + \frac{1}{\rho_0}\Delta_x p = fv, \tag{18b}$$
$$\Delta_t v + \frac{1}{\rho_0}\Delta_y p = -fu, \tag{18c}$$
$$\Delta_t p + \gamma p_0(\Delta_x u + \Delta_y v) = 0. \tag{18d}$$

Apply Δ_x to (18bb), Δ_y to (18bc), Δ_t to (18bd), and make the appropriate substitution. This gives us

$$\Delta_t\Delta_t p = \frac{\gamma p_0}{\rho_0}(\Delta_x\Delta_x p + \Delta_y\Delta_y p) - f\gamma p_0(\Delta_x v - \Delta_y u). \tag{19}$$

If $f = 0$, then this discretization is equivalent to a scalar wave discretization. Hence, in the absence of Coriolis forces, the discretization scheme (18b) is compatible with the discrete Higdon NRBCs (as modified below).

Continuing our derivation, we apply Δ_y to (18bb) and Δ_x to (18bc), then subtract and combine terms to get

$$\Delta_t\left(\Delta_y u - \Delta_x v\right) = f\left(\Delta_y v + \Delta_x u\right). \tag{20}$$

We then substitute (18bd) into this result to get

$$\Delta_t(\Delta_y u - \Delta_x v) = -\frac{f}{\gamma p_0}\Delta_p. \tag{21}$$

If we apply Δ_t to (19) and incorporate (21), we get

$$\Delta_t\left[\Delta_t\Delta_t p - \frac{\gamma p_0}{\rho_0}\left(\Delta_x\Delta_x p + \Delta_y\Delta_y p\right) + f^2 p\right] = 0. \tag{22}$$

Thus, the quantity inside the brackets is constant from one time step to the next. Since this equation applies to our initial state, then the quantity within the brackets must initially be zero and thus remain zero always; hence

$$\Delta_t\Delta_t p = \frac{\gamma p_0}{\rho_0}(\Delta_x\Delta_x p + \Delta_y\Delta_y p) - f^2 p. \tag{23}$$

If we expand our $\Delta_{[x,y,t]}$ symbols into their corresponding shift operators and apply them to the state variable p, we see that (23) is actually

$$\frac{p_{i,j}^{n+2} - 2p_{i,j}^n + p_{i,j}^{n-2}}{(2\delta t)^2} = \frac{\gamma p_0}{\rho_0}\left(\frac{p_{i+2,j}^n - 2p_{i,j}^n + p_{i-2,j}^n}{(2\delta x)^2} + \frac{p_{i,j+2}^n - 2p_{i,j}^n + p_{i,j-2}^n}{(2\delta y)^2}\right) - f^2 p_{i,j}^n. \tag{24}$$

This equation is the standard second-order centered-difference scheme for the Klein–Gordon equation *on a double-sized grid*. Hence, the appropriate discretization for the Higdon scheme is not (11) but

$$\partial_t \simeq \frac{I - S_t^{-2}}{2\delta t}, \quad \partial_x \simeq \frac{I - S_x^{-2}}{2\delta x}. \tag{25}$$

Remark 1. This scheme cannot resolve the shortest wavelengths resolvable by the interior scheme. Rather, it treats a particular wave as an overlap of two waves, each with twice the wavelength of the original wave, and it resolves the waves

Author's personal copy

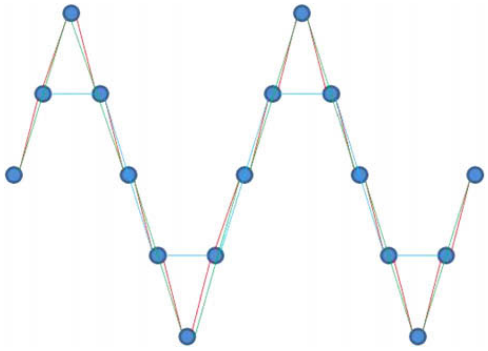

Fig. 2. A computational wave (red) interpreted as an overlap of two longer-wavelength waves (green and blue). (For interpretation of the references to colour in this figure legend, the reader is referred to the web version of this article.)

on alternating time steps (see Fig. 2). Despite this apparent deficiency, we have observed no loss of stability even in a contrived example featuring such short wavelengths.

7. Numerical example

Let us consider a simple numerical example. We look at a square domain 10 km on each side, subdividing it into a 100×100 computational domain with the Higdon-like NRBCs on all four sides (see Fig. 1). We define the NRBC for all four state variables, because we use a centered-difference discretization. A one-sided discretization scheme would enable us to use a natural boundary condition on one side or another, but previous experiments have shown that such a scheme is unstable.

Using a mean atmoshperic density of $1.2\ \mathrm{kg/m^3}$ and pressure of $1.01 \times 10^5\ \mathrm{N/m^2}$ [12], a Coriolis value of $f = 7.292116 \times 10^{-5}$ rad/s [28], and zero advection, our initial condition is a cosine bubble in the center of the domain

$$\begin{aligned} p^0_{x,y} &= \begin{cases} p_0\left(1 + \frac{\cos\left(\frac{\pi d}{2r}\right)}{100}\right) & : d \le r \\ p_0 & : \text{otherwise} \end{cases} \\ \rho^0_{x,y} &= \begin{cases} \rho_0\left(\frac{p^0_{x,y}}{p_0}\right)^{\frac{c_v}{c_p}} & : d \le r \\ \rho_0 & : \text{otherwise}, \end{cases} \end{aligned} \tag{26}$$

where

$$\begin{aligned} d &= \sqrt{(x - x_C)^2 + (y - y_C)^2}, \\ r &= 1\ \mathrm{km}, \end{aligned}$$

and x_C and y_C denote the center of the domain. The initial condition for ρ is chosen to maintain constant potential temperature with the pressure perturbation [3]. For comparison, our reference solution domain is 30 km wide and 30 km high, with the domain of interest in the center. We define the normalized error norm for each state variable η as

$$E_\eta = \frac{\sqrt{\sum_{i=1}^{N_x}\sum_{j=1}^{N_y}(\eta_J(i,j) - \eta_0(i,j))^2}}{\sqrt{\sum_{i=1}^{N_x}\sum_{j=1}^{N_y}\eta_0(i,j)^2}}, \tag{27}$$

where N_x, N_y are the number of grid points in the x and y directions, respectively, η_J is a solution state variable using the J-order NRBC, and η_0 is the reference solution. We divide by the norm of η_0 so that the error norms of each state variable are approximately the same order of magnitude. Our time step is set to 90% of the maximum δt allowed by the CFL limit, where the CFL limit is

$$\left(C_0\frac{\delta t}{\delta x}\right)^2 + \left(C_0\frac{\delta t}{\delta y}\right)^2 \le 1, \tag{28}$$

where $C_0 = \sqrt{\gamma p_0/\rho_0}$ is the acoustic wave speed. Using the discretization scheme (18b), we run the simulation up to $t = 24$, long enough for the primary wave to exit the computational domain with the wave trough just passing through the corners. Figs. 3–6 show the four state variables at the end of the run for $J = 10$. Fig. 7 compares the state variable u at the end of the $J = 1$ and $J = 10$ cases; note the dramatic reduction in spurious reflection in the $J = 10$ case. (We have observed here that if the order is increased beyond $J = 10$, numerical instabilities appear which destroy the solution. We observed the same instability for $J > 10$ in developing the numerical examples of [25] for the Klein–Gordon equation. The cause is unknown but is

Author's personal copy

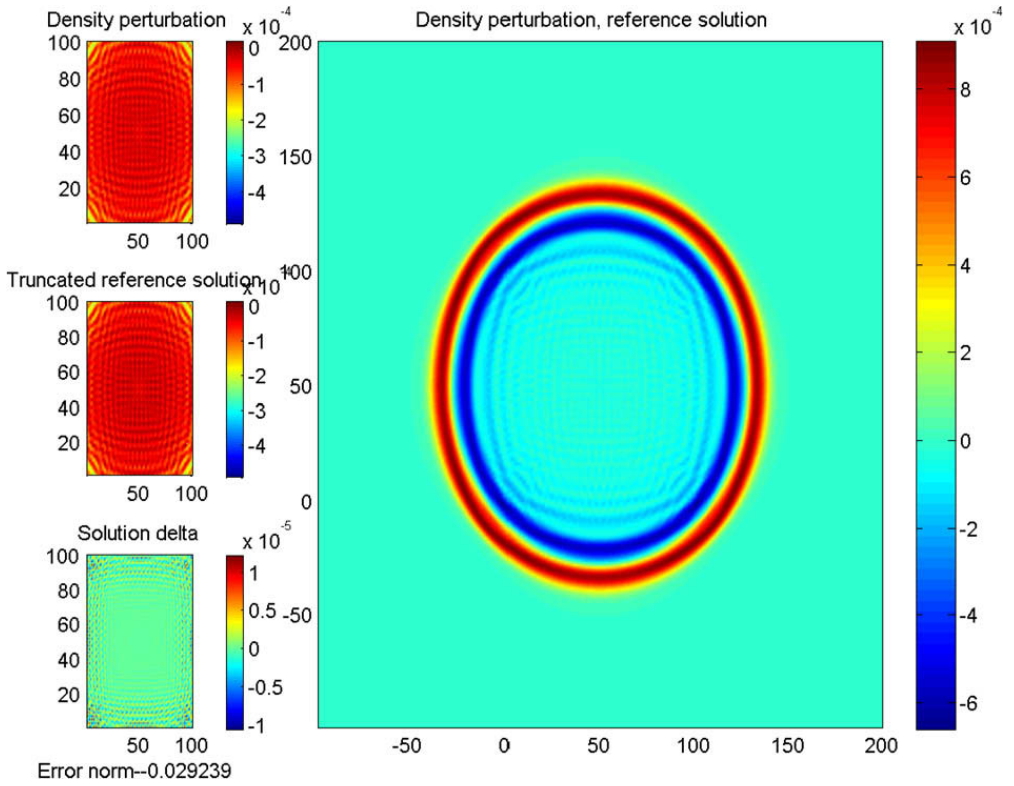

Fig. 3. The solution for the density ρ using $J = 10$. (TL) Computed solution using NRBCs. (Right) Reference solution. (CL) Reference solution domain corresponding to NRBC solution domain. (BL) Delta between computed and reference solutions, with error norm computed by (27).

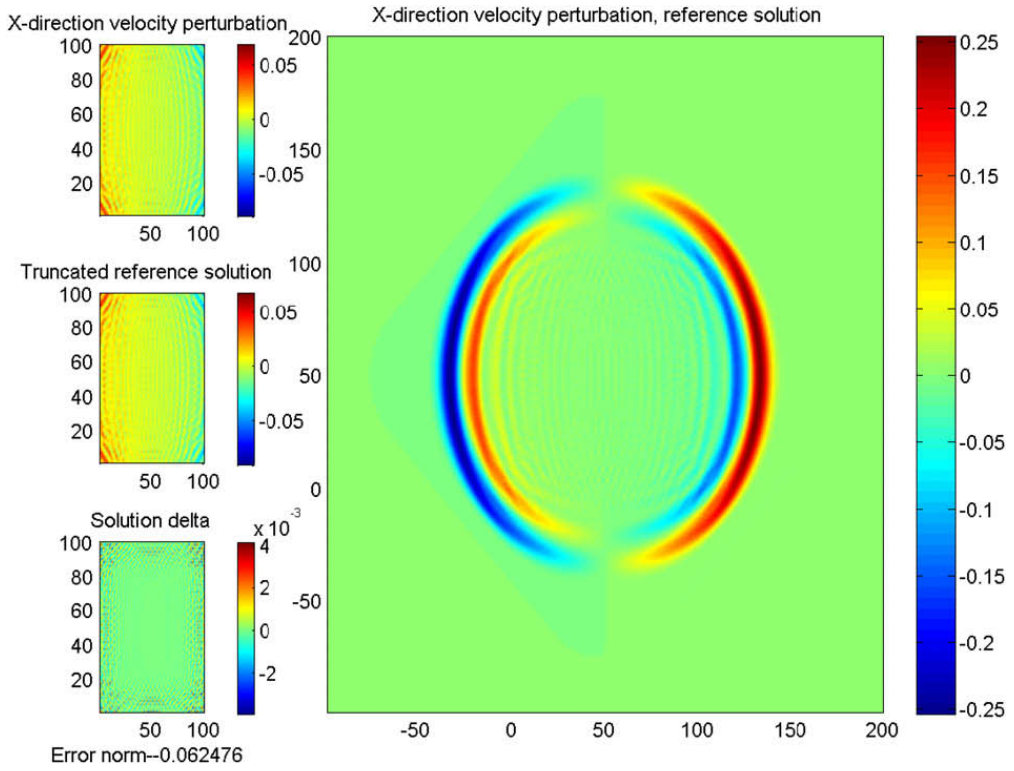

Fig. 4. The solution for the x-direction velocity u using $J = 10$. (TL) Computed solution using NRBCs. (Right) Reference solution. (CL) Reference solution domain corresponding to NRBC solution domain. (BL) Delta between computed and reference solutions, with error norm computed by (27).

suspected to be due to round-off errors associated with small individual values in the summation of the high-order derivatives.) Table 1 and Fig. 8 shows the error norms (27) for each state variable as J goes from 1 to 10.

Author's personal copy

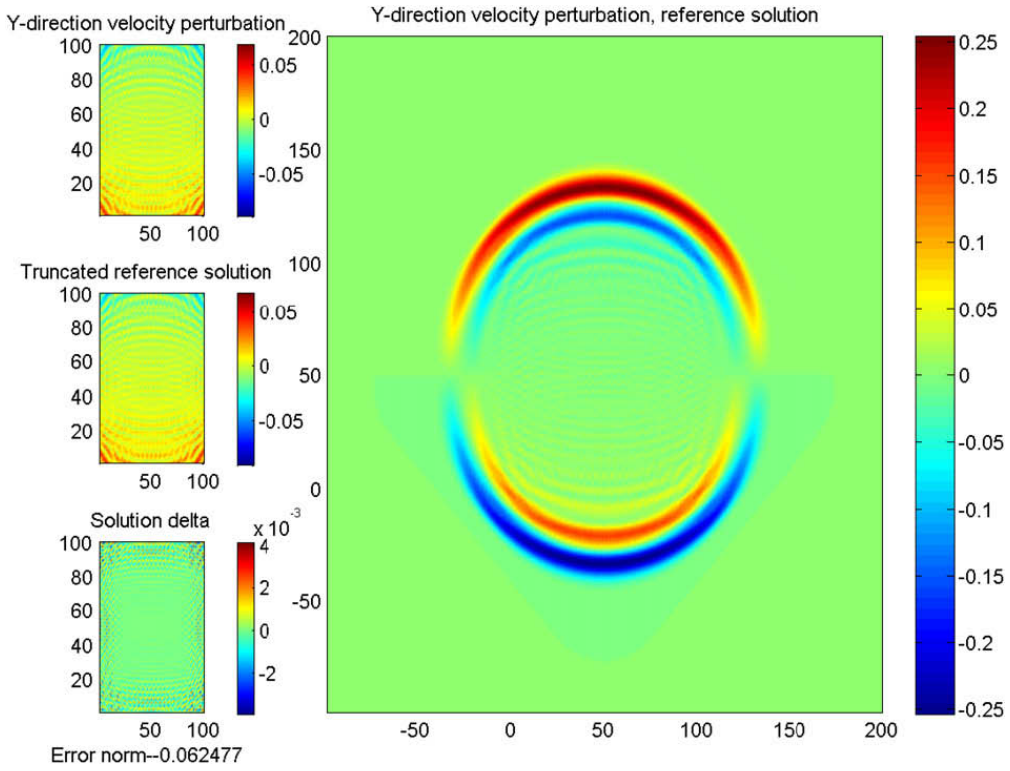

Fig. 5. The solution for the y-direction velocity v using $J = 10$. (TL) Computed solution using NRBCs. (Right) Reference solution. (CL) Reference solution domain corresponding to NRBC solution domain. (BL) Delta between computed and reference solutions, with error norm computed by (27).

One note about the time step: we have found experimentally that if δt is set to exactly the CFL limit, then the error norm for $J = 10$ is only approximately 55% the $J = 1$ error norm. On the other hand, if we use exactly half the CFL limit for our δt, then the error norm reduction is on the order of 99.5%. We chose 90% of the maximum δt as a compromise between increased accuracy and increased time step size. The reason for the improved NRBC performance with smaller δt is unknown, but it may be similar to the "safety factor" recommended by Tannehill et al. for the non-linear Navier–Stokes equations (see p. 627 of [27]). Analysis of this particular aspect of the NRBC performance will be addressed in future research.

8. Areas for further research

The preceding example demonstrates, in a limited setting, that high-order Higdon NRBCs are compatible with the linearized Euler equations. However, there are far more areas to explore in this implementation. The following list shows some of the areas available for future research, some of which are currently under investigation by the authors:

1. Thorough investigation of the long-time stability for large J.
2. Extending the scheme to the case of the linearized Euler equations with Coriolis and nonzero mean flow (advection).
3. Thorough investigation of the relationship between the time step size (the Courant number) and the NRBC performance for large J.
4. Extending the scheme to the full 3-D system, including the effects of gravity.
5. Implementing the scheme with auxiliary variables, using high-order finite differences and finite elements, using both the Givoli–Neta AV formulation [10] and the Hagstrom–Warburton variation [11].
6. Extending the scheme to permit incoming waves, for example, in a nested mesoscale model.
7. Experimenting with the use of the NRBC with the non-linear Euler equations (1) in the computational domain. (Need to find a stable interior scheme-NRBC combination.)

9. Conclusion

In this paper, we have shown that Higdon-type NRBCs are compatible with the linearized Euler equations with Coriolis and zero mean flow. These NRBCs provide greater accuracy (reduced spurious reflection) than the basic Sommerfeld boundary condition. A prototypical implementation was developed, and a numerical example demonstrating the capabilities of the scheme was provided.

Author's personal copy

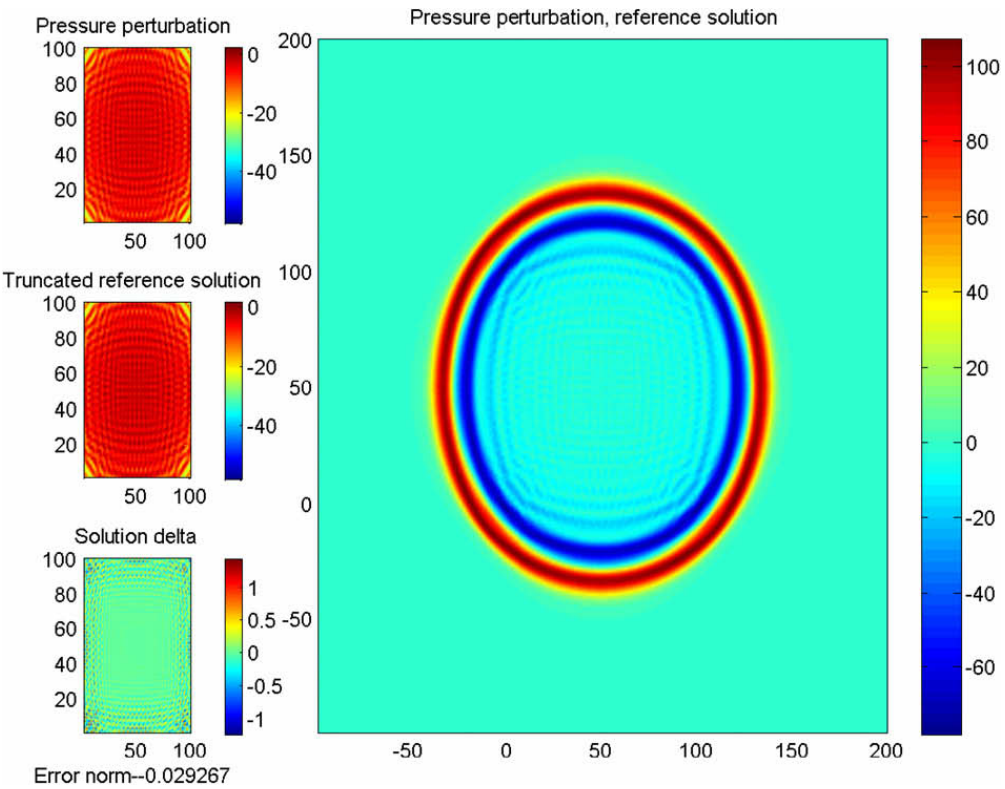

Fig. 6. The solution for the pressure p using $J = 10$. (TL) Computed solution using NRBCs. (Right) Reference solution. (CL) Reference solution domain corresponding to NRBC solution domain. (BL) Delta between computed and reference solutions, with error norm computed by (27).

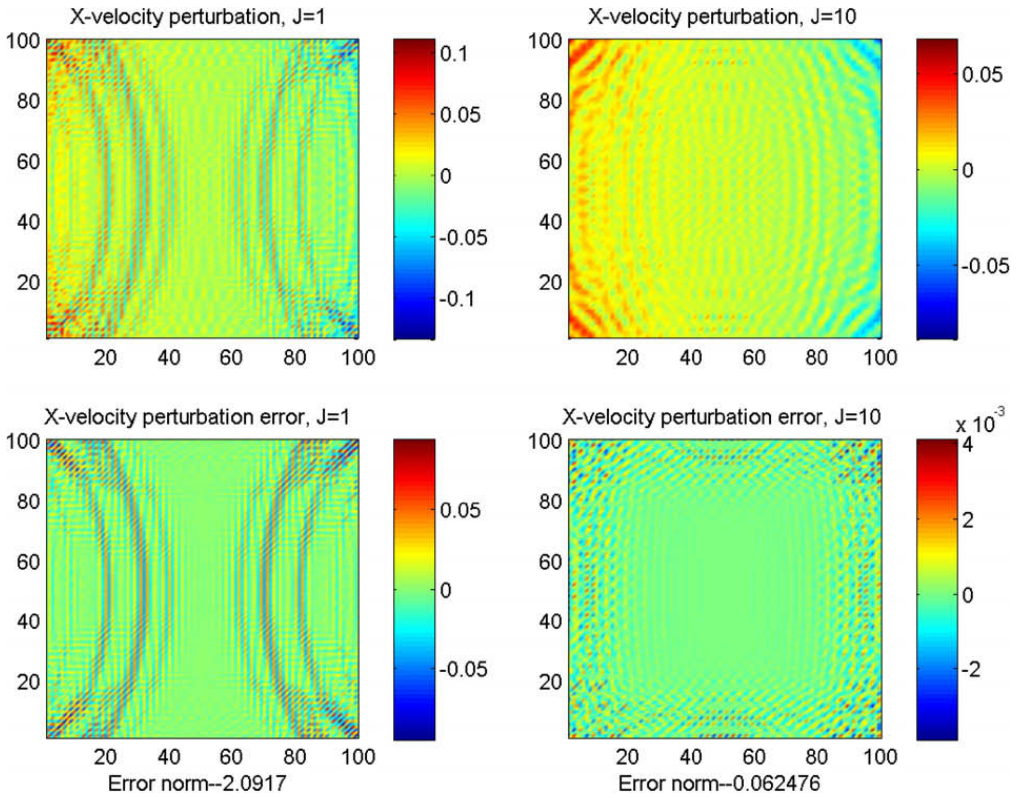

Fig. 7. A comparison of solutions for u using $J = 1$ and $J = 10$. (TL) Computed solution using $J = 1$. (TR) Computed solution using $J = 10$. (BL) Delta between reference solution and $J = 1$ solution, with error norm computed by (27). (BR) Delta between reference solution and $J = 10$ solution, with error norm computed by (27).

Author's personal copy

Table 1
Error norms (27) for $J \in 1 \ldots 10$ with discretization scheme (18b).

J	E_ρ	E_u	E_v	E_p
1	1.5191	2.0917	2.0917	1.5205
2	0.42052	0.61777	0.61777	0.42092
3	0.18953	0.30055	0.30054	0.18971
4	0.11677	0.19766	0.19766	0.11689
5	0.081815	0.14588	0.14588	0.081893
6	0.061569	0.11564	0.11564	0.061628
7	0.048183	0.095798	0.095797	0.04823
8	0.03908	0.082285	0.082284	0.039118
9	0.033036	0.071617	0.071617	0.033067
10	0.029239	0.062476	0.062477	0.029267

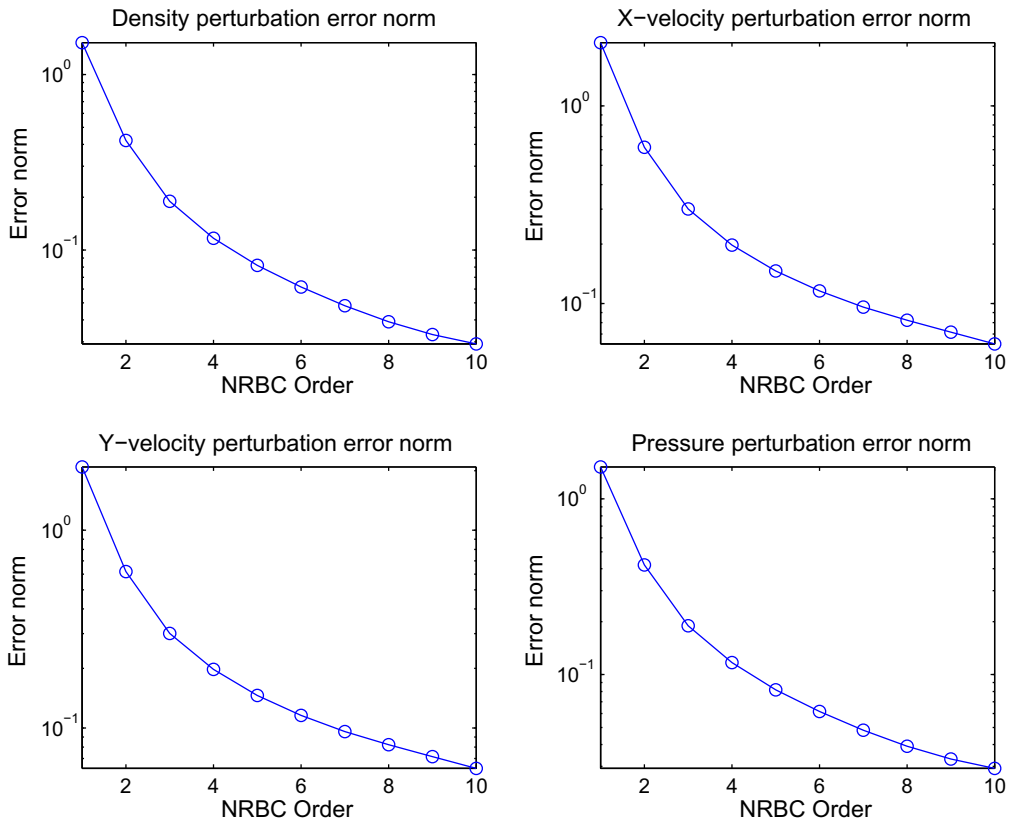

Fig. 8. Logarithmic plot of state variable error norms (27) for $J \in 1 \ldots 10$ with discretization scheme (18b). (TL) Error norms for ρ. (TR) Error norms for u. (BL) Error norms for v. (BR) Error norms for p.

Acknowledgements

The authors would like to express their appreciation to the Naval Postgraduate School for its support of this research. The first author is also indebted to the Air Force Institute of Technology for its support. Finally, the authors thank the reviewers for their helpful suggestions and comments.

References

[1] J. Bérenger, A perfectly matched layer for the absorption of electromagnetic waves, J. Comput. Phys. 114 (1994) 185–200.
[2] J. Dea, F. Giraldo, B. Neta, High-Order Higdon Non-Reflecting Boundary Conditions for the Linearized Euler Equations, NPS-MA-07-001, Naval Postgraduate School, Monterey, CA, 2007.
[3] D. Durran, Numerical Methods for Wave Equations in Geophysical Fluid Dynamics, Springer, New York, 1999.
[4] B. Engquist, A. Majda, Absorbing boundary conditions for the numerical simulation of waves, Math. Comput. 31 (1977) 629–651.
[5] B. Engquist, A. Majda, Radiation boundary conditions for acoustic and elastic wave calculations, Commun. Pure Appl. Math. 32 (1979) 313–357.
[6] F. Giraldo, M. Restelli, A study of spectral element and discontinuous Galerkin methods for mesoscale atmospheric modeling: equation sets and test cases, J. Comput. Phys. 227 (2008) 3849–3877.

Author's personal copy

[7] D. Givoli, B. Neta, High-Order Higdon Non-Reflecting Boundary Conditions for the Shallow Water Equations, NPS-MA-02-001, Naval Postgraduate School, Monterey, CA, 2001.
[8] D. Givoli, B. Neta, High-order non-reflecting boundary conditions for dispersive waves, Wave Motion 37 (2003) 257–271.
[9] D. Givoli, B. Neta, High-order non-reflecting boundary conditions for the dispersive shallow water equations, J. Comput. Appl. Math. 158 (2003) 49–60.
[10] D. Givoli, B. Neta, High-order non-reflecting boundary scheme for time-dependent waves, J. Comput. Phys. 186 (2003) 24–26.
[11] T. Hagstrom, T. Warburton, A new auxiliary variable formulation of high-order local radiation boundary conditions: corner compatibility conditions and extension to first-order systems, Wave Motion 39 (2004) 327–338.
[12] D. Halliday, R. Resnick, Fundamentals of Physics, third ed., John Wiley and Sons, New York, 1988. Extended.
[13] R. Higdon, Absorbing boundary conditions for difference approximations to the multi-dimensional wave equation, Math. Comput. 47 (1986) 437–459.
[14] R. Higdon, Initial-boundary value problems for linear hyperbolic systems, SIAM Rev. 28 (1986) 177–217.
[15] R. Higdon, Numerical absorbing boundary conditions for the wave equation, Math. Comput. 49 (1987) 65–90.
[16] R. Higdon, Radiation boundary conditions for elastic wave propagation, SIAM J. Numer. Anal. 27 (1990) 831–869.
[17] R. Higdon, Absorbing boundary conditions for elastic waves, Geophysics 56 (1991) 231–241.
[18] R. Higdon, Absorbing boundary conditions for acoustic and elastic waves in stratified media, J. Comput. Phys. 101 (1992) 386–418.
[19] R. Higdon, Radiation boundary conditions for dispersive waves, SIAM J. Numer. Anal. 31 (1994) 64–100.
[20] F. Hu, On absorbing boundary conditions for linearized Euler equations by a perfectly matched layer, J. Comput. Phys. 129 (1996) 201–219.
[21] F. Hu, A. Stable, Perfectly matched layer for linearized Euler equations in unsplit physical variables, J. Comput. Phys. 173 (2001) 455–480.
[22] F. Hu, A perfectly matched layer absorbing boundary condition for linearized Euler equations with a non-uniform mean flow, J. Comput. Phys. 208 (2005) 469–492.
[23] D. Kröner, Absorbing boundary conditions for the linearized Euler equations in 2-D, Math. Comput. 57 (1991) 153–167.
[24] I. Navon, B. Neta, M. Hussaini, A perfectly matched layer approach to the linearized shallow water equations models, Month. Weather Rev. 132 (2004) 1369–1378.
[25] B. Neta, V. van Joolen, J. Dea, D. Givoli, Application of high-order Higdon non-reflecting boundary conditions to linear shallow water models, Commun. Numer. Methods Eng., in press, published online at www.interscience.wiley.com, doi:10.1002/cnm.1044.
[26] I. Orlanski, A simple boundary condition for unbounded hyperbolic flows, J. Comput. Phys. 21 (1976) 251–269.
[27] J. Tannehihll, D. Anderson, R. Pletcher, Computational Fluid Mechanics and Heat Transfer, second ed., Taylor & Francis, Washington, DC, 1997.
[28] D. Vallado, Fundamentals of Astrodynamics and Applications, second ed., Microcosm Press, El Segundo, CA, 2001.
[29] V. Van Joolen, Application of Higdon non-reflecting boundary conditions to shallow water models, Ph.D dissertation, Naval Postgraduate School, Monterey, CA, 2003.
[30] V. Van Joolen, D. Givoli, B. Neta, High-order non-reflecting boundary conditions for dispersive waves in cartesian, cylindrical and spherical coordinate systems, Int. J. Comput. Fluid Dyn. 17 (2003) 263–274.
[31] V. Van Joolen, B. Neta, D. Givoli, A stratified dispersive wave model with high-order non-reflecting boundary conditions, Comput. Math. Appl. 48 (2004) 1167–1180.
[32] V. Van Joolen, B. Neta, D. Givoli, High-order Higdon-like boundary conditions for exterior transient wave problems, Int. J. Numer. Methods Eng. 63 (2005) 1041–1068.